BRCA1 deficiency in skin epidermis leads to selective loss of hair follicle stem cells and their progeny

Panagiota A. Sotiropoulou,[1,5,6] Andrea E. Karambelas,[1,5] Maud Debaugnies,[1] Aurelie Candi,[1] Peter Bouwman,[2] Virginie Moers,[1] Tatiana Revenco,[1] Ana Sofia Rocha,[1] Kiyotoshi Sekiguchi,[3] Jos Jonkers,[2] and Cedric Blanpain[1,4,6]

[1]IRIBHM (Institut de Recherche Interdisciplinaire en Biologie Humaine et Moleculaire), Université Libre de Bruxelles, Brussels 1070, Belgium; [2]Division of Molecular Pathology, Cancer Systems Biology Center, The Netherlands Cancer Institute, Amsterdam 1066 CX, The Netherlands; [3]Institute for Protein Research, Osaka University, Osaka 565-0871, Japan; [4]WELBIO (Walloon Excellence in Life Sciences and Biotechnology), Université Libre de Bruxelles, Brussels 1070, Belgium

The accurate maintenance of genomic integrity is essential for tissue homeostasis. Deregulation of this process leads to cancer and aging. BRCA1 is a critical mediator of this process. Here, we performed conditional deletion of *Brca1* during epidermal development and found that BRCA1 is specifically required for hair follicle (HF) formation and for development of adult HF stem cells (SCs). Mice deficient for *Brca1* in the epidermis are hairless and display a reduced number of HFs that degenerate progressively. Surprisingly, the interfollicular epidermis and the sebaceous glands remain unaffected by *Brca1* deletion. Interestingly, HF matrix transient amplifying progenitors present increased DNA damage, p53 stabilization, and caspase-dependent apoptosis compared with the interfollicular and sebaceous progenitors, leading to hyperproliferation, apoptosis, and subsequent depletion of the prospective adult HF SCs. Concomitant deletion of *p53* and *Brca1* rescues the defect of HF morphogenesis and loss of HF SCs. During adult homeostasis, BRCA1 is dispensable for quiescent bulge SCs, but upon their activation during HF regeneration, *Brca1* deletion causes apoptosis and depletion of *Brca1*-deficient bulge SCs. Our data reveal a major difference in the requirement of BRCA1 between different types of epidermal SCs and progenitors and during the different activation stages of adult HF SCs.

[*Keywords*: Brca1; stem cells; skin epidermis; DNA damage and repair; homeostasis; cancer]

Supplemental material is available for this article.

Received September 24, 2012; revised version accepted November 26, 2012.

The maintenance of genome integrity is crucial for tissue development and homeostasis, and failure to preserve genome maintenance may result in cancer, accelerated aging, or both (Garinis et al. 2008; Hoeijmakers 2009). All living cells are continuously challenged by DNA damage caused by external stress and highly reactive by-products of cellular metabolism or during DNA replication. Several highly conserved DNA repair mechanisms exist in eukaryotic cells to recognize and repair the multiple types of DNA damage (Hoeijmakers 2001; Sancar et al. 2004; Harper and Elledge 2007). The most deleterious type of DNA lesions are double-strand breaks (DSBs), which are repaired by homologous recombination (HR) during the S and G2/M phases of the cell cycle and by nonhomologous end-joining (NHEJ) during G0/G1. HR is an error-free DNA repair mechanism, as it uses the intact sister strand as a template to repair DNA DSBs, thereby accurately preserving genetic information, while NHEJ ligates together the broken ends and thus potentially results in small deletions, nucleotide changes, or chromosomal translocations (Lombard et al. 2005). Mutations in either of these pathways can result in premature aging, neurodegeneration, and increased risk of cancer (Hakem 2008).

The skin epidermis is a stratified epithelium consisting of the interfollicular epidermis (IFE) and its appendages: the hair follicles (HFs) and the associated sebaceous glands (SGs) (Blanpain and Fuchs 2006; Sotiropoulou and Blanpain 2012). The homeostasis of these different epidermal compartments is ensured by different pools of resident stem cells (SCs), each of which is located in a different niche (Blanpain and Fuchs 2009). Multipotent HF SCs reside in the permanent region of the HF called the bulge region and are responsible for the cyclic regeneration of the HF. The maintenance of the IFE is ensured by

[5]**These authors contributed equally to this work.**
[6]**Corresponding authors**
E-mail cedric.blanpain@ulb.ac.be
E-mail psotirop@ulb.ac.be
Article published online ahead of print. Article and publication date are online at http://www.genesdev.org/cgi/doi/10.1101/gad.206573.112.

the presence of multiple units of proliferation containing long-lived SCs and short-lived committed progenitors (Clayton et al. 2007; Mascre et al. 2012). Finally, the turnover of the SG and the maintenance of the infundibulum, the part of the HF connected to the IFE, are mediated by resident progenitors located in this region of the HF and expressing different markers, such as MTS24, Lrig1, and Lgr6 (Nijhof et al. 2006; Jensen et al. 2009; Snippert et al. 2010). The epidermis is the outer barrier of the body and thus is constantly exposed to mutagenic assaults such as UV or ionizing radiation (Blanpain et al. 2011). Since epidermal SCs renew in the adult skin of animals throughout their life, they are at high risk of accumulating DNA damage and mutations that can impair their function. We showed recently that adult bulge SCs are strongly resistant to DNA damage-induced cell death through their higher expression of the anti-apoptotic protein Bcl2 and through accelerated DNA repair activity mediated by NHEJ (Sotiropoulou et al. 2010). As the different types of SCs in the epidermis exhibit distinct turnover rates (Sotiropoulou and Blanpain 2012), the higher activity of NHEJ found in adult bulge SCs may reflect their relative quiescence (Blanpain et al. 2011), which poises them to use NHEJ preferentially to repair their DNA. It is not clear whether the different SCs located in the same tissue rely on specific DNA repair mechanisms at a given stage of development.

Recent studies have shown that adult SCs from distinct tissues respond differently to DNA damage (Blanpain et al. 2011). Adult mouse hematopoietic SCs, similar to bulge SCs, are more resistant to DNA damage-induced cell death than their downstream progenitors (Mohrin et al. 2010), while human neonatal cord blood SCs are more sensitive to DNA damage (Milyavsky et al. 2010), suggesting that either the species or the stage of SC ontogeny may dictate the response to DNA damage. Since the different developmental stages are characterized by distinct proliferation rates, it is possible that HR and NHEJ are differentially used during morphogenesis and homeostasis to preserve the fitness and the pool of SCs at distinct stages of development and activation.

Using conditional ablation of *Brca1* during both embryonic development and adult homeostasis, we assessed the relative importance of BRCA1 in the specification and maintenance of the different pools of SCs present in the mouse epidermis. BRCA1 not only is a critical mediator of HR (Huen et al. 2010), but also dictates the choice between HR and NHEJ by displacing 53BP1 from the ends of the DSBs (Bunting et al. 2010) or by blocking 53BP1 accumulation (Chapman et al. 2012), enabling resection of the break and initiation of HR. Interestingly, we found that the distinct types of epidermal SCs respond differently to *Brca1* deletion. While the IFE and SG remain mostly unaffected upon *Brca1* deletion, BRCA1 is essential for HF bulge SC development and homeostasis. Upon *Brca1* deletion, transient amplifying matrix cells undergo p53-dependent apoptosis, which induces continuous activation, extensive proliferation, and cell death of the prospective bulge SCs, leading to their rapid exhaustion and failure to sustain the homeostasis of the HF lineages.

Results

Brca1 *deletion in the epidermis during embryonic development results in a decreased number of HFs*

BRCA1, a key mediator of DNA repair, is expressed in every compartment of the skin epidermis, including the IFE, SG, and HF (Supplemental Fig. 1). To define the importance of BRCA1 during epidermal development, we performed conditional deletion of *Brca1* specifically in the skin epidermis of *K14Cre/Brca1*$^{fl/fl}$ (*Brca1* cKO [conditional knockout]) mice, which express the Cre recombinase in the developing epidermis from embryonic day 12 (E12) and thereafter (Vasioukhin et al. 2001). At E17, the epidermis is stratified, and P-cadherin-positive HF rudiments are already visible at different stages of their development (placodes, hair germs, hair pegs, and HFs) (Rhee et al. 2006). Quantification of the number of embryonic HFs at E17 demonstrated that *Brca1* cKO mice present a decrease of 50% in the number of HFs, which are in a less advanced stage of maturation compared with wild-type epidermis (Fig. 1A–C).

To determine whether the decrease in the number of HFs in *Brca1* cKO mice is due to a defect in the signaling pathways instructing HF fate, we studied the activation of the Wnt/β-catenin pathway, which is the first signal required for HF morphogenesis (Blanpain and Fuchs 2006). As shown in Figure 1D, nuclear β-catenin was observed in the developing placode and surrounding mesenchyme in the *Brca1* cKO mice, demonstrating that the loss of epidermal appendages is not due to a defect in the Wnt/β-catenin signaling pathway. Similarly, Lhx2 (Fig. 1E), a transcription factor that controls HF development and acts downstream from Wnt and Hedgehog signaling during HF morphogenesis (Rhee et al. 2006), is also normally expressed in the HFs of *Brca1* cKO epidermis, showing that *Brca1* deletion does not alter the expression of well-known HF determinants.

Another possibility is that the HF progenitors die by apoptosis as a result of their inability to repair endogenous DNA damage, leading to a decrease in the number of HFs. To investigate this possibility, we assessed the expression of active Caspase-3 in the epidermis at E17. We found that the *Brca1* cKO epidermis contains many active caspase-3-positive cells, which were localized mainly in the HF rudiments (Fig. 1F,G). To determine whether apoptosis is the main cause of the decreased number of HFs in *Brca1* cKO mice, we administered the pan-caspase inhibitor Z-VAD-FMK to pregnant mice from E10 to E17. Interestingly, administration of Z-VAD-FMK completely rescued the number of embryonic HFs in the *Brca1* cKO mice (Fig. 1H), demonstrating that the decreased number of HFs following *Brca1* deletion in the embryonic epidermis was indeed caused by apoptosis.

Deletion of Brca1 *in the epidermis results in degeneration of HFs, leading to a hairless phenotype*

At birth, *Brca1* cKO mice are healthy and do not differ from their wild-type littermates. However, while hair starts to be visible around postnatal day 6 (P6) in wild-

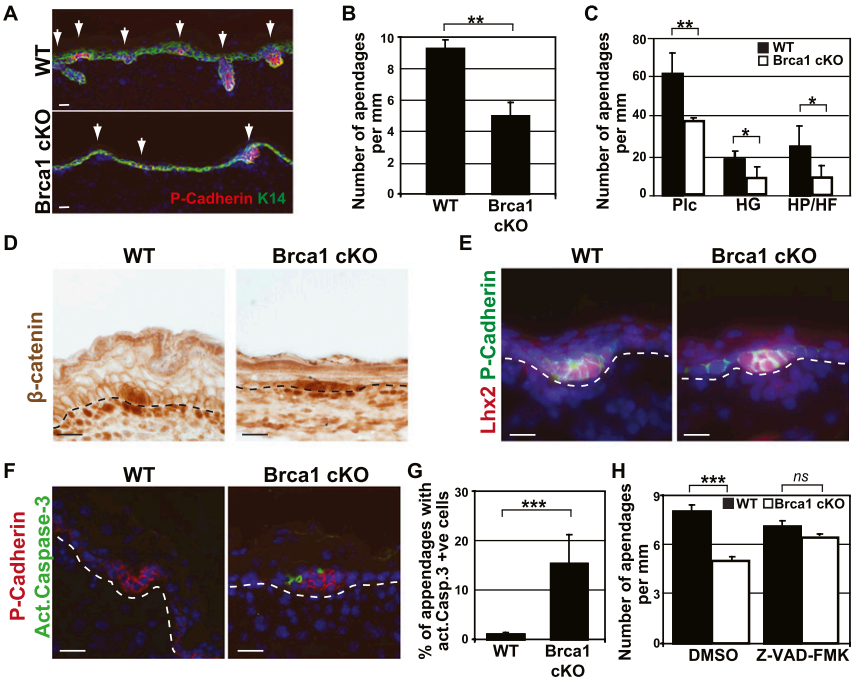

Figure 1. *Brca1* deletion during embryonic development results in a reduction of the number of HFs. (*A*) Representative images of the epidermis of E17 wild-type (WT) and *K14Cre;Brca1*$^{fl/fl}$ (*Brca1* cKO) mice. Arrows indicate epidermal rudiments stained here with P-Cadherin in red. (*B*) Quantification of the number of embryonic HFs per millimeter of skin in wild-type and *Brca1* cKO mice, showing the decrease of the number of rudiments in the cKO epidermis (n = 100 10× optical fields analyzed in five different mice). (*C*) Quantification of the type of epidermal rudiments in wild-type and *Brca1* cKO animals. (*D*) β-Catenin expression in wild-type and *Brca1* cKO mice. (*E*) Lhx2 expression in E17 wild-type and *Brca1* cKO epidermis. Note the comparable expression pattern of the two early HF markers in wild-type and *Brca1* cKO animals. (*F*) Apoptosis in wild-type and *Brca1* cKO mice as determined by active caspase-3 immunofluorescence. (*G*) Quantification of apoptotic cells in immunofluorescence images of wild-type and *Brca1* cKO mice, showing the high levels of apoptosis in the epidermis of cKO mice (n = 50 10× optical fields analyzed in five different mice). (*H*) Quantification of the embryonic HFs in wild-type and *Brca1* cKO mice at E17 upon daily injections to the pregnant female of the pan-caspase inhibitor Z-VAD-FMK or DMSO as a control from E10 to E17. Note the rescue of the phenotype in the cKO mice exposed to the caspase inhibitor (n = 50 10× optical fields analyzed in seven different mice). Error bars represent the SEM. Bars, 20 μm. (Plc) Placodes; (HG) hair germ; (HP) hair peg.

type mice, *Brca1* cKO mice remain hairless (Fig. 2A) and never develop hair, showing that absence of hair in *Brca1* cKO mice is not the result of a delay in HF development. Since the cKO mice do initially develop about half the HFs of wild-type mice during epidermal morphogenesis, we performed a temporal analysis of the postnatal skin to investigate the fate of the surviving HFs. As shown in Figure 2B, BRCA1-deficient HFs were smaller, thinner, and more twisted than their wild-type counterparts. Moreover, after the first month of age, the lower part of the HFs underneath the SG progressively degenerated and was lost before the second postnatal month. Quantification of HF density (Fig. 2C) revealed that the lower part of the HFs (Fig. 2C, solid black line) was progressively lost in *Brca1* cKO epidermis, and at 2 mo of age, almost no lower HFs could be seen in BRCA1-deficient mice, while the upper part (Fig. 2C, dotted black line) was maintained.

To determine why BRCA1-deficient HFs never make visible hair shafts, we analyzed the expression of HF differentiation markers associated with the different HF lineages. Surprisingly, despite the absence of macroscopic hair shafts, markers of the different HF lineages, including the inner root sheath and the precortex markers, were detected in BRCA1-deficient HFs (Fig. 2D) except for the very few cells expressing the medulla markers AE15 and Desmocollin-2, demonstrating that the absence of visible hair in BRCA1 deficiency did not result from the inability of HF cells to undergo terminal differentiation.

Brca1 *deficiency does not impair renewal and differentiation of the IFE and SG*

To investigate whether the other epidermal lineages, including the IFE and the SG, are also affected in *Brca1* cKO mice, we investigated the expression of the differentiation markers of the IFE. The expression of K1, K10, and loricrin is unaffected in BRCA1-deficient epidermis. Similarly, the expression of the isthmus progenitor marker MTS24 and Lrig1, a marker of the junctional zone progenitors, is largely unaffected in *Brca1* cKO epidermis, and functional SGs could be detected following Oil Red O staining (Fig. 3). Altogether, these data indicate that the functional defect of BRCA1 deficiency in the epidermis is restricted to the lower part of the HFs.

Brca1 *deficiency leads to a higher level of DNA damage, p53 stabilization, and apoptosis in the lower HF cells compared with the rest of the epidermis*

To define why the lower HF is more sensitive to the loss of BRCA1 than the rest of the epidermis, we analyzed whether HFs present more DNA damage than the other epidermal cells. To this end, we investigated the expression of the DNA damage markers γH2AX, which localizes at unrepaired DSBs (Bonner et al. 2008), and 53BP1, which also clusters in foci at sites of DNA damage (Schultz et al. 2000). Under physiological conditions, nuclear γH2AX foci are very rare in wild-type epidermis, although some cells of the HF matrix presenting one or

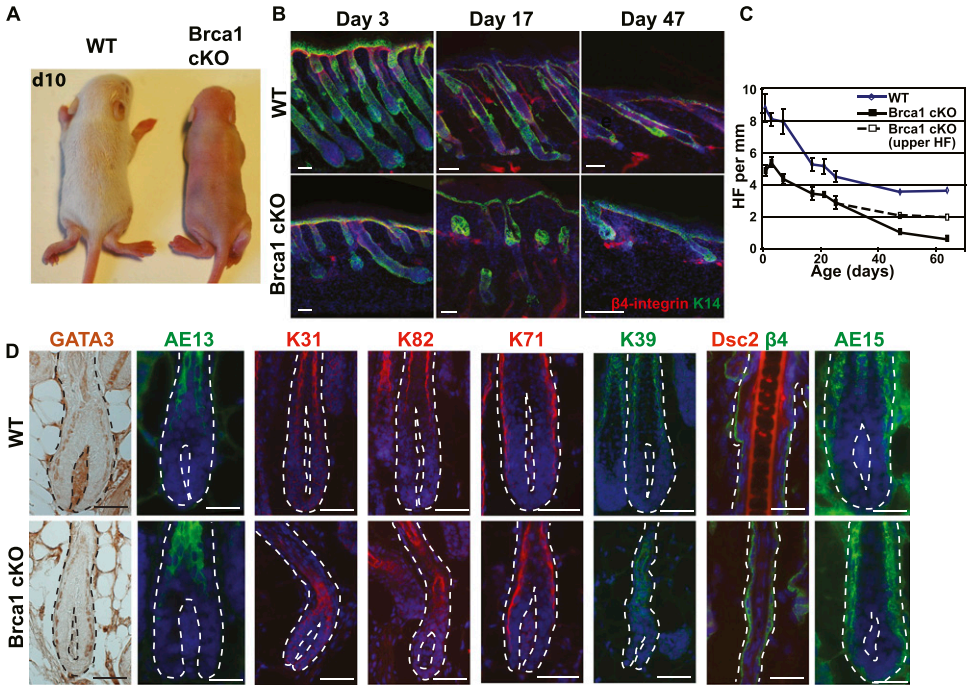

Figure 2. *Brca1* deletion in the epidermis leads to congenital alopecia and progressive degeneration of the HFs. (*A*) Macroscopic pictures of wild-type (WT) and *Brca1* cKO mice at P10 (d10) illustrating the complete absence of hair in *Brca1* cKO mice. (*B*) Kinetics of the HF cycle in wild-type and cKO epidermis. Note the progressive degradation of the lower part of the HFs under the SG. (*C*) Quantification of the number of HFs per millimeter of skin. For the cKO mice, the solid line represents the number of complete HFs, while the dotted line indicates the number of HFs irrespective of the presence of a lower part ($n = 50$ 10× optical fields analyzed in five different mice). (*D*) Immunofluorescence analysis of the HF differentiation markers illustrating the presence of cells expressing HF differentiation markers in the *Brca1* cKO mice, except from the medulla markers AE15 and Dsc2. Error bars represent the SEM. Bars, 20 μm. (Dsc2) Desmocollin 2.

a few γH2AX foci can be detected (apoptotic cells that also express a high level of γH2AX, albeit not in foci, have been excluded from the quantification) (Fig. 4A,B). In contrast, several BRCA1-deficient lower HF cells present γH2AX foci, and these cells usually contain more γH2AX foci per cell (Fig. 4A–C). Likewise, 53BP1 clusters are more abundant in BRCA1-deficient lower HFs compared with the other parts of the *Brca1*-null epidermis and with wild-type lower HFs (Fig. 4D), supporting the notion that the greater sensitivity of the lower part of the HFs to *Brca1* deletion is related to the increased accumulation of DNA damage in these cells.

DNA damage triggers p53 stabilization, which in turn mediates a transient cell cycle arrest to allow the cells to repair DNA damage, and if the damage is too extensive or cannot be repaired, this triggers apoptosis (Riley et al. 2008). To determine whether *Brca1* deletion in the epidermis induces p53 stabilization, we performed immunostaining for p53 and active Caspase-3 in skin sections of wild-type and *Brca1* cKO mice (Fig. 4E,G) and quantified the number of positive cells in the different epidermal compartments (Fig. 4F,H). As for γH2AX and 53BP1 foci, the number of p53 and active Caspase-3-positive cells is increased in the epidermis of *Brca1* cKO mice, especially in the lower part of the BRCA1-deficient HFs (Fig. 4F,H). These results suggest that a higher number of unrepaired DSBs specifically at the lower part of the *Brca1* cKO HFs leads to increased p53 stabilization and apoptosis.

Given the progressive degeneration of the lower HFs, we investigated the number, proliferation, and apoptosis of matrix progenitors. While the number of matrix cells in wild-type mice remains constant from P10 to P14, the

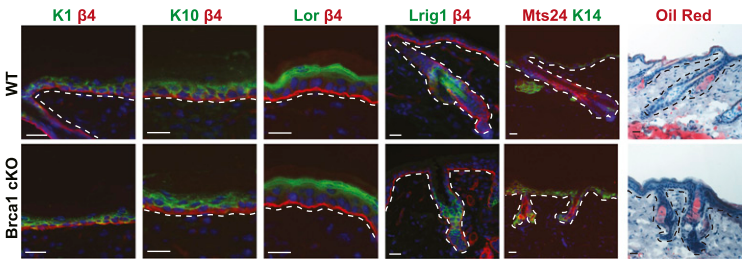

Figure 3. The IFE and SGs are unaffected upon *Brca1* deletion. Immunofluorescence analysis of markers of the IFE and SG showing the normal expression of IFE and SG differentiation markers as well as their progenitor cells in *Brca1* cKO mice. Note the comparable expression of all of the factors in wild-type (WT) and cKO mice. Bars, 20 μm.

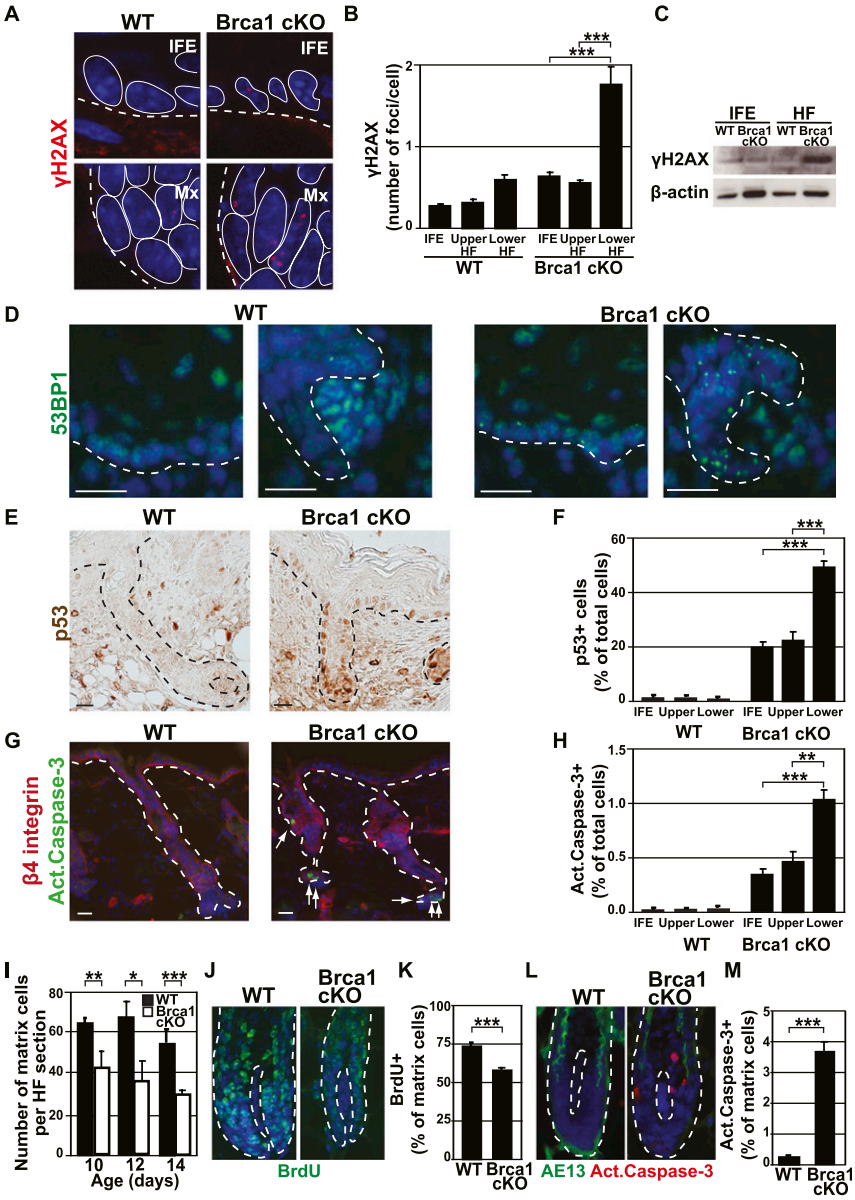

Figure 4. The HF matrix exhibits a higher level of DNA damage, p53 expression, and apoptosis upon *Brca1* deletion. (*A*) Representative confocal microscope images of γH2AX foci in the IFE (*top* panels) or the matrix (*bottom* panels) of P10 wild-type (WT) and *Brca1* cKO mice. The dotted lines indicate the border of the epidermis with dermis, while the solid lines delineate the individual cells. (*B*) Quantification of γH2AX foci in immunofluorescent images as presented in *A*. Four-hundred-fifty IFE cells, 550 upper HF cells, and 1500 lower HF cells belonging to 10 different HFs from each one of three independent mice were counted. (*C*) Western blot analysis of γH2AX expression in FACS-isolated IFE and lower HF cells from wild-type and *Brca1* cKO mice. B-Actin was used as loading control. (*D*) Representative images of 53BP1 expression in the IFE (*left* panels) and matrix (*right* panels) of wild-type and *Brca1* cKO mice. Note the abundance of 53BP1 foci in the lower HFs of the cKO mice. (*E,F*) Immunohistochemistry images and quantification of the p53^{+} cells in the distinct compartments of the epidermis. While present throughout the tissue, note the higher number of cells and the stronger expression of p53 in the lower part of the HFs. (*G,H*) Immunofluorescent images and quantification of the apoptotic cells in the distinct compartments of the epidermis using active caspase-3 staining. (*I*) Quantification of the number of HF matrix cells in longitudinal sections in wild-type and *Brca1* cKO mice at the indicated time points, illustrating the rapid decrease in the matrix size in the *Brca1* cKO animals ($n = 20$ HFs encompassing between 600 and 1750 cells from three different mice). (*J,K*) Representative images and quantification of proliferating cells in the matrix of P10 wild-type and *Brca1* cKO mice using BrdU labeling after 24-h BrdU pulse. Note the lower proliferation rate of the matrix in the *Brca1* cKO mice ($n = 20$ HFs encompassing between 700 and 1200 cells from each of three individual mice). (*L,M*) Representative images and quantification of apoptotic cells in the matrix in P10 wild-type and *Brca1* cKO mice using active caspase-3 immunofluorescence and AE13 to delineate the limits of the matrix ($n = 20$ HFs encompassing between 600 and 1750 cells from three different mice). Error bars represent the SEM. Bars, 20 μm. (Mx) matrix.

number of matrix cells decreases in *Brca1* cKO animals (Fig. 4I). To define the reason for this decrease in matrix size, we analyzed proliferation and cell death in these transient amplifying cells in wild-type and *Brca1* cKO mice. BrdU incorporation was decreased by 30% (Fig. 4J,K), and a high number of active Caspase-3-positive cells (Fig. 4L,M) was observed in the BRCA1-deficient matrix cells. These data clearly show that the progressive reduction in the pool of HF transient amplifying cells in BRCA1-deficient epidermis is the consequence of their increased cell death, which cannot be compensated for by increased proliferation of surviving cells.

Absence of slow-cycling adult HF bulge SCs in BRCA1-deficient epidermis

The lower part of the HF is maintained by slow-cycling multipotent SCs located in the permanent portion of the HF called the bulge, located underneath the SG. Bulge SCs are responsible for the regeneration of the new HFs at each hair cycle and express high levels of CD34 (Trempus et al. 2003; Blanpain et al. 2004; Tumbar et al. 2004). Immunostaining and FACS analysis show the complete absence of bulge SCs expressing CD34 in the adult *Brca1* cKO mice (Fig. 5A,B). Since CD34, the only

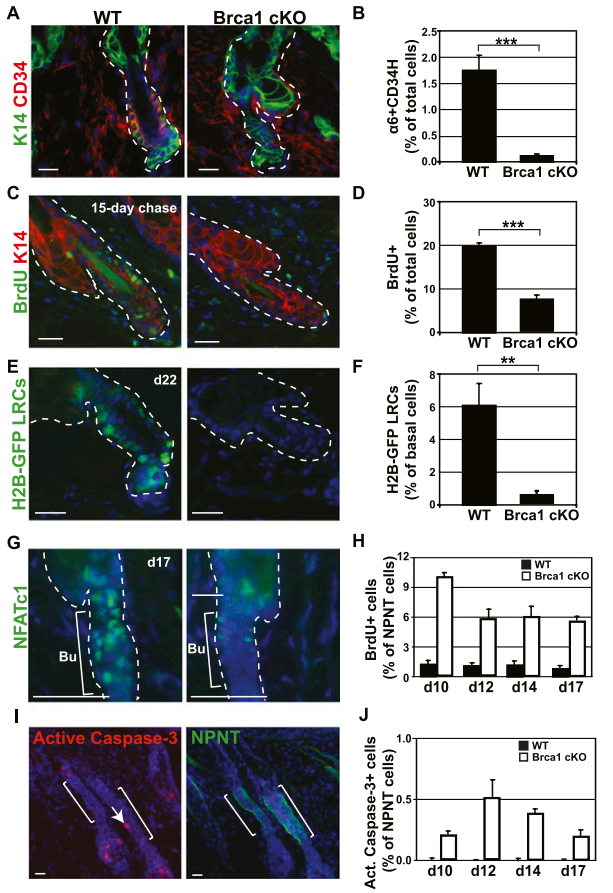

Figure 5. Absence of quiescent adult HF SCs in BRCA1-deficient epidermis. (*A*,*B*) Representative images and quantification by FACS of adult bulge SCs labeled with CD34 in P47 wild-type (WT) and *Brca1* cKO mice, demonstrating the complete absence of bulge SCs in the *Brca1* cKO animals. (*C*,*D*) Representative images and quantification by FACS of the LRCs after BrdU pulse from P3 to P5 and 15 d of chase, demonstrating the reduction of LRCs in *Brca1* cKO epidermis (n = 4 mice for each condition). (*E*) Representative images of H2B-GFP expression in P22 (d22) *Brca1*$^{fl/fl}$*;K5tTA;H2B-GFP* (wild-type) and *K14Cre;Brca1*$^{fl/fl}$*; K5tTA;H2B-GFP* (*Brca1* cKO) mice treated continuously with doxycycline from E18.5, confirming the lack of H2B-GFP LRCs in the prospective bulge area of the *Brca1* cKO epidermis. (*F*) Quantification by FACS of the number of H2B-GFP$^+$ cells in wild-type and cKO mice as described in *E*. A FACS gate was set for living basal cells that present a level of fluorescence indicating that they accomplished less than four divisions. (*G*) Immunofluorescence analysis of Nfatc1, a marker of quiescence, showing the significant reduction of Nfatc1 expression in the prospective bulge area of *Brca1* cKO mice. (*H*) Quantification of proliferating cells in the prospective bulge region, delineated with NPNT immunostaining, of wild-type and *Brca1* cKO mice at the indicated ages using BrdU labeling after 24-h BrdU pulse (n = 1000 cells from each of two individual mice). (*I*) Representative images of active caspase-3 and NPNT immunostaining on serial sections of a P12 (d12) *Brca1* cKO mouse. The lines indicate the bulge areas as determined by NPNT expression, and the arrow is pointing to an apoptotic bulge SC. (*J*) Quantification of apoptotic prospective bulge SCs, as presented in *I*, at the indicated ages. Note the peak of apoptosis at P12 (d12) (n = 10,000 cells from each of two individual mice per time point). Error bars represent the SEM. Bars, 20 μm. (Bu) Bulge.

specific marker for bulge SCs, begins to be expressed around P21 (Blanpain et al. 2004), we could not determine whether bulge SCs were never specified in the *Brca1* cKO mice or were initially normally specified but subsequently lost.

It has been shown recently that the slow-cycling property of prospective bulge SCs occurs early during HF morphogenesis (Nowak et al. 2008). To determine whether the prospective bulge SCs were specified and then lost during HF morphogenesis, we assessed whether slow-cycling cells could be detected in BRCA1-deficient epidermis using label retention studies. To this end, mice were pulsed with BrdU from P3 to P5 and chased for 2 wk. As shown in Figure 5, C and D, label-retaining cells (LRCs) are concentrated in the bulge area of the wild-type mice, while very few BrdU LRCs are detected in the *Brca1* cKO epidermis. However, because BrdU causes a certain level of DNA damage and *Brca1* cKO mice exhibit defects in DNA repair, we cannot exclude the possibility that BrdU administration may induce apoptosis in the prospective bulge SCs. To circumvent the problem of the potential BrdU toxicity, we used *K5-tTA/TetO-H2B-GFP* mice to perform label retention studies with H2B-GFP, which has been successfully used to mark slow-cycling bulge SCs in adult mice (Tumbar et al. 2004) as well as during HF morphogenesis (Nowak et al. 2008). Doxycycline was continuously administered to *K5-tTA;TetO-H2B-GFP;K14Cre;Brca1*$^{fl/fl}$ mice to induce the chase of H2B-GFP starting at E18.5, and the mice were analyzed at P22. As previously reported (Nowak et al. 2008), most H2B-GFP-high LRCs are located in the bulge area of wild-type mice, consistent with the acquisition of the slow-cycling properties of the prospective bulge SCs during HF morphogenesis (Fig. 5E). In sharp contrast, there were almost no H2B-GFP-high LRCs in *Brca1* cKO epidermis (Fig. 5E). Quantification of the level of H2B-GFP fluorescence by flow cytometry showed that <1% of cells in the *Brca1* cKO epidermis underwent fewer than four divisions, contrasting with the 6% of H2B-GFP LRCs observed in wild-type mice (Fig. 5F). Moreover, NFATc1, another marker of the prospective quiescent bulge SCs (Horsley et al. 2008), was initially detected in *Brca1* cKO mice (data not shown) but was lost over time (Fig. 5G), further suggesting that prospective bulge SCs progressively lost their quiescence feature.

To determine the cellular mechanisms leading to the absence of adult CD34 bulge SCs in *Brca1*-deficient epidermis, we excluded ectopic differentiation (Supplemental Fig. 2A) and performed a detailed temporal analysis of proliferation and apoptosis in the prospective bulge region of *Brca1* cKO mice during HF morphogenesis (Fig. 5H–J; Supplemental Fig. 2B). To delineate the prospective bulge area, we used nephronectin (NPNT), an extracellular matrix protein expressed in the restricted region of the upper part of the lower outer root sheath cells that includes the prospective bulge SCs from early postnatal days (Supplemental Fig. 2C; Fujiwara et al. 2011). As shown in Figure 5H, the prospective bulge SCs in *Brca1* cKO mice exhibited a fivefold to 10-fold higher rate of BrdU incorporation compared with their wild-type lit-

termates, with a peak of proliferation at P10 (10% of BrdU-positive cells). At this time point, only very few prospective bulge SCs (<0.2%) were caspase-3-positive (Fig. 5J), suggesting that at P10, bulge SCs actively proliferate to compensate for the high amount of cell death in HF matrix TA cells (10–20 times more active caspase-3-positive cells compared with the prospective bulge SCs). Proliferation remained higher in *Brca1*-deficient prospective bulge cells throughout HF morphogenesis, while apoptosis peaked at P12 (0.5% of active caspase-3-positive cells), 2 d after the peak of proliferation, and decreased to 0.2% thereafter (Fig. 5J).

Collectively, these data indicate that *Brca1*-deficient prospective bulge SCs initially proliferate to compensate for the massive apoptosis of HF TA matrix cells, and this hyperproliferation is accompanied by a slight but significant increase in their apoptosis that contributes to the premature exhaustion of these progenitor cells, leading to the absence of adult bulge SCs in *Brca1*-deficient epidermis.

Deletion of p53 *rescues the hairless phenotype and the lack of bulge SCs in the BRCA1-deficient epidermis*

Our data indicate that unrepaired DNA damage, p53 stabilization, and apoptosis of HF transient amplifying matrix cells could be responsible for the hairless phenotype and the absence of bulge SCs in adult mice. To test this possibility functionally, we performed conditional deletion of *p53* together with *Brca1* deletion. Interestingly, concomitant deletion of *p53* completely rescues HF development and the specification of adult bulge SCs in BRCA1-deficient epidermis (Fig. 6A–C), demonstrating that p53-dependent cell death of the lower HF is the main mechanism leading to the absence of HF differentiation and the lack of HF bulge SCs in *Brca1*-deficient epidermis.

Deletion of Brca1 *during adult homeostasis results in the progressive depletion of* Brca1*-deficient bulge SCs during HF regeneration*

To define whether BRCA1 is also essential for the maintenance of adult HF bulge SCs, we performed conditional deletion of *Brca1* in the adult epidermis, when the pool of bulge SCs is already established. To this end, we administered 15 mg of tamoxifen (TAM) over 2 wk to 4-wk-old *K5CreER;Brca1$^{fl/fl}$;Rosa-YFP* mice to delete *Brca1* specifically in the adult epidermis (adult *Brca1* cKO) (Fig. 7A).

After TAM administration, only very rare BRCA1^{+} cells could be detected by immunohistochemistry in *K5CreER;Brca1$^{fl/fl}$;Rosa-YFP*-treated mice (Fig. 7B). Quantification of the number of cells expressing YFP revealed that 75% of the bulge SCs and 50% of the other epidermal cells had undergone recombination at the Rosa26 locus (Supplemental Fig. 3A,B). To determine more precisely the frequency of TAM-induced *Brca1* recombination, we quantified by real-time PCR the relative frequency of

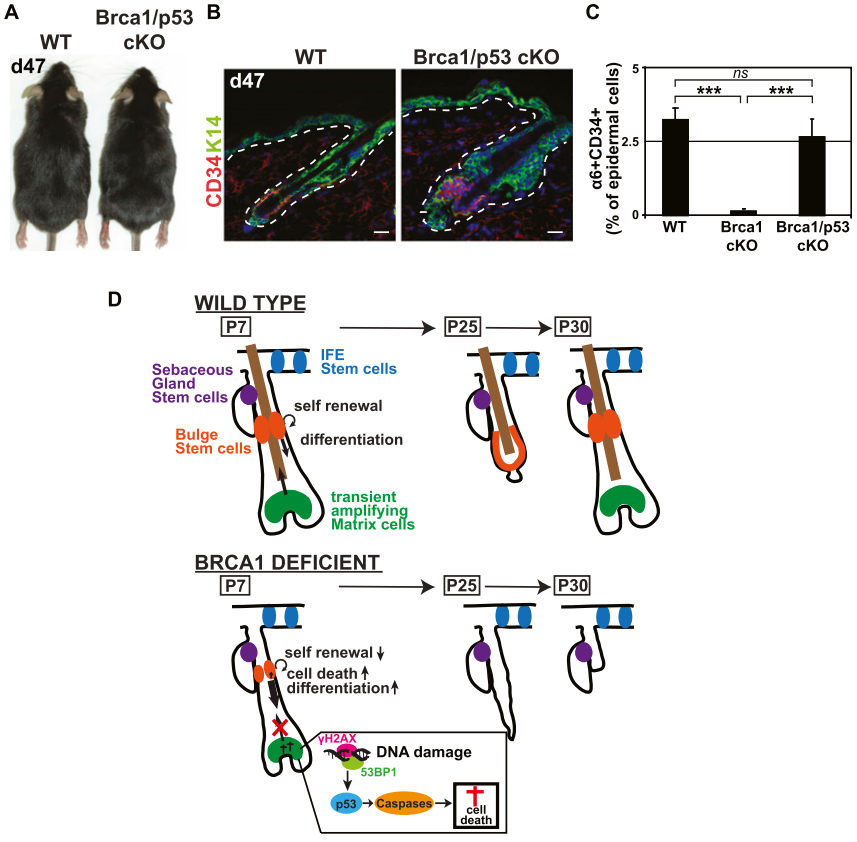

Figure 6. *p53* deletion rescues HF differentiation and the loss of adult HF SCs. (*A*) Image of P47 (d47) *Brca1$^{fl/fl}$;p53$^{fl/fl}$* (wild-type [WT]) and *K14Cre;Brca1$^{fl/fl}$;p53$^{fl/fl}$* (*Brca1/p53* cKO) mice, demonstrating the rescue of the hair phenotype in *Brca1* cKO mice by concomitant inactivation of *p53*. (*B,C*) Representative images and quantification by FACS of the adult HF bulge SC in P47 (d47) wild-type and *Brca1;p53* double cKO mice, showing that p53 rescues the SC phenotype of BRCA1-deficient mice. (*D*) Model of functional consequences of *Brca1* deletion in the skin epidermis. *Brca1* deletion in skin epidermis leads to increased DNA damage, p53 stabilization, and caspase-dependent apoptosis in the HF transient amplifying matrix cells, inducing compensatory proliferation of the bulge HF SCs to replenish the dying matrix progenitors. This hyperproliferation is accompanied by a defect in the balance between self-renewal and differentiation of HF bulge SC progenitors and concomitant apoptosis, leading to their exhaustion and the degeneration of the lower (n = 4 animals for each condition). Error bars represent the SEM. Bars, 20 μm.

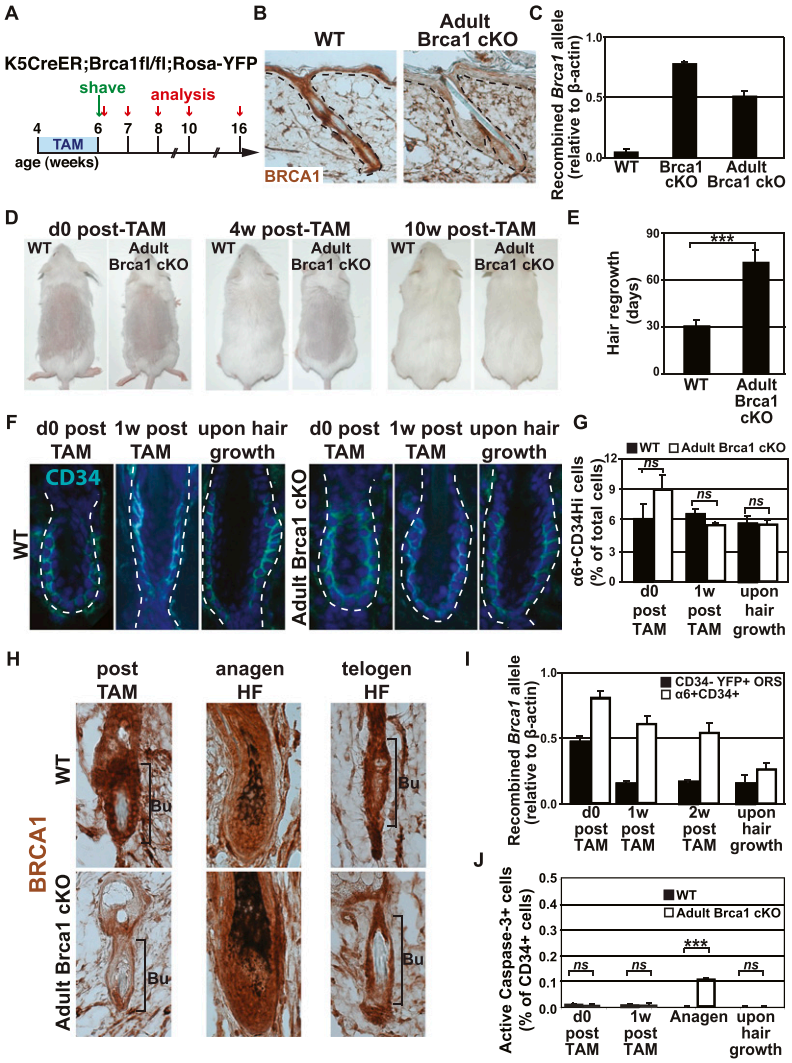

Figure 7. *Brca1* deletion in adult HF bulge SCs leads to their progressive depletion. (*A*) Scheme presenting the strategy used to induce *Brca1* deletion in adult epidermis and to monitor its functional consequences. (*B*) Immunohistochemistry of BRCA1 after TAM administration to wild-type (WT) and *K5CreER;Brca1*$^{fl/fl}$*;Rosa-YFP* (adult *Brca1* cKO) mice. (*C*) Quantitative PCR analysis of the expression of the recombined *Brca1* allele after TAM administration performed on FACS-isolated keratinocytes. Results are presented relative to β-actin expression ($n = 5$ animals for each condition). (*D*) Representative pictures of wild-type and adult *Brca1* cKO mice just after, 4 wk after, and 10 wk after TAM administration. (*E*) Histogram showing the time required before observing hair regrowth in wild-type and adult *Brca1* cKO mice after TAM administration ($n = 12$ mice for each condition). (*F,G*) Representative immunofluorescence and FACS quantification of CD34 expression in wild-type and adult *Brca1* cKO mice immediately and 1 wk after TAM administration and upon hair regrowth ($n = 5$ mice for each condition). (*H*) BRCA1 immunohistochemistry in the bulge and the newly formed HFs after TAM administration and upon hair growth. Note the BRCA1 expression in the newly formed HFs and in the bulge after hair growth in adult *Brca1* cKO TAM-treated mice. (*I*) Quantitative PCR analysis of the expression of the recombined *Brca1* allele on FACS-sorted CD34$^+$ and YFP$^+$ outer root sheath cells at the indicated time points after TAM administration. Results are presented relative to β-actin expression. Note the reduction in the expression of the recombined *Brca1* allele in the bulge SCs of adult *Brca1* cKO TAM-treated mice ($n = 5$ animals for each condition). (*J*) Quantification of apoptosis in the bulge SCs as determined by active caspase-3 immunostaining in wild-type and adult *Brca1* cKO mice at the indicated time points. Note the increase of bulge CD34 SC apoptosis during anagen ($n = 6000$ cells for each of two mice per condition). Error bars represent the SEM. Bars, 20 μm. (Bu) Bulge; (ORS) outer root sheath.

recombined and nonrecombined *Brca1* floxed alleles in FACS-sorted epidermal populations. Following TAM administration, the frequency of the nonrecombined allele strongly decreased, while the frequency of the recombined *Brca1* allele almost reached the level found upon constitutive epidermal *Brca1* deletion (*K14Cre;Brca1*$^{fl/fl}$ mice) (Fig. 7C; Supplemental Fig. 3C). Surprisingly, *K5CreER;Brca1*$^{fl/fl}$*;Rosa-YFP* TAM-induced mice regrew hair after shaving, albeit with some delay compared with the control mice treated with TAM (Fig. 7D,E). To determine the effect of *Brca1* deletion in adult bulge SCs, we analyzed the expression of CD34 by immunostaining and FACS. The similar frequency of CD34-expressing cells in wild-type and *K5CreER;Brca1*$^{fl/fl}$*;Rosa-YFP* mice at different time points following TAM administration, in which most adult bulge SCs were initially deficient for BRCA1 (Fig. 7F,G), suggests that either BRCA1 is not essential for adult bulge SC maintenance or *Brca1*-deficient bulge SCs were outcompeted by the few remaining nonrecombined *Brca1* wild-type bulge SCs during the next stage of HF regeneration. Indeed, while after TAM administration to *K5CreER;Brca1*$^{fl/fl}$*;Rosa-YFP* mice, bulge SCs were mostly BRCA1-negative, in the newly formed HFs, they were always BRCA1-positive, and 10 wk post-TAM, most of the bulge SCs expressed BRCA1 (Fig. 7H). Moreover, a time-course analysis of the expression of the *Brca1* recombined allele by quantitative PCR showed that the frequency of the recombined allele progressively decreased over time during HF regeneration, and the newly formed HFs contained a very low level of the *Brca1* recombined allele (Fig. 7I), demonstrating the requirement of BRCA1 for adult HF regeneration and the progressive loss of adult *Brca1*-deficient bulge SCs over time. Analysis of apoptosis of bulge SCs following *Brca1* deletion revealed that at the end of TAM administration, when most *Brca1*-deficient bulge SCs were in their resting stage, no increase in apoptosis was detected in CD34 bulge cells (Fig. 7J). However, when

HFs entered anagen and bulge SCs were activated, increased frequency of active caspase-3 was observed in CD34-expressing cells from *K5CreER;Brca1$^{fl/fl}$;Rosa-YFP*-treated mice (Fig. 7J). Collectively, these data show that BRCA1 is dispensable for adult bulge SC maintenance during the quiescent stage, but BRCA1 is required during the active stage that accompanies HF regeneration.

Discussion

Our study shows that BRCA1 deficiency in the epidermis impairs HF morphogenesis and the development and homeostasis of adult HF bulge SCs, while the upper part of the epidermis—the IFE and SG—remains unaffected. A combination of direct and indirect consequences of *Brca1* deletion cooperate to trigger the loss of HF SCs. The increased p53-mediated apoptosis of HF matrix TA cells induces intense proliferation of prospective bulge SCs to compensate for the loss of HF progenitors. This hyperproliferation must be accompanied by a defect in the balance between self-renewal and differentiation, shifting the equilibrium toward enhanced HF differentiation in order to replenish the rapidly dying HF TA matrix cells. In addition, the low but persistent apoptosis in the rapidly proliferating prospective bulge cells further contributes to their exhaustion and depletion and to the subsequent degeneration of the lower part of the HFs (Fig. 6D). Likewise, during skin homeostasis, BRCA1 is not essential for adult HF bulge SCs during their quiescent stage, possibly because quiescent bulge SCs preferentially use NHEJ to maintain their genomic integrity (Sotiropoulou et al. 2010; Symington and Gautier 2011). However, upon activation of bulge SCs during HF regeneration, *Brca1* deletion leads to apoptosis and elimination of *Brca1*-deficient bulge SCs.

The progressive degeneration of HFs upon *Brca1* deletion results from p53-dependent apoptosis of matrix cells. Simultaneous deletion of *p53* completely rescued HF morphogenesis and differentiation as well as the loss of adult bulge SCs in BRCA1-deficient epidermis. It has been shown that *Brca1* deletion in a *p53*-null background alleviates the phenotype of BRCA1 deficiency, rescuing mice from embryonic lethality but resulting in premature aging and tumorigenesis (Cao et al. 2003). BRCA1 is a multifunctional protein (Huen et al. 2010), and the effects of the *p53* deletion in BRCA1-deficient cells may vary between different tissues. It is therefore possible that *p53* deletion may only partly or transiently rescue the observed HF SC phenotype. The demonstration that HF morphogenesis and differentiation are at least initially fully rescued in *Brca1/p53* double cKO mice demonstrates the essential role of p53-mediated cell death in this phenotype. The preferential apoptosis of matrix cells committed to the inner cells of the future hair shaft results in the absence of the tight and aligned packing of premedulla cells, required to form the rigid multilayer sheath of the hair shaft (Birbeck and Mercer 1957; O'Guin et al. 1992).

While conditional deletion of *Brca1* using *K14Cre* has been previously performed, it did not result in the absence of HF morphogenesis or differentiation (Liu et al. 2007; Rottenberg et al. 2007). However, the *K14Cre* line used in these experiments displays mosaic expression in the skin (Jonkers et al. 2001), thereby enabling HF morphogenesis by cells that escaped *Brca1* deletion. Outcompetition of recombined cells by nonrecombined wild-type cells usually occurs when deletion of genes essential for SC renewal is induced in a mosaic manner. In contrast, the *K14Cre* used in our study is not mosaically expressed and results in Cre-mediated recombination in all epidermal cells starting at E12 (Vasioukhin et al. 1999), preventing the emergence of nonrecombined *Brca1*-positive cells that could contribute to hair morphogenesis.

The most important question arising from our study is why the upper part of the epidermis—the IFE and SG—is unaffected by *Brca1* deletion, while the HFs degenerate. In the wild-type mice, BRCA1 is equally expressed in all epidermal compartments, showing that the differential response to *Brca1* deletion cannot be explained by the absence of BRCA1 expression from the upper part of the epidermis. The exquisite sensitivity of HF matrix cells upon *Brca1* deletion is reminiscent of its role in the early cortical progenitors during brain development (Pulvers and Huttner 2009). Which mechanism could underpin the differential requirement of BRCA1 in different types of SCs? Are HF matrix progenitors more sensitive or are IFE and SG SCs more resistant to *Brca1* deletion? It is possible that higher metabolic activity or lower reactive oxygen species (ROS) buffering might lead to more extensive endogenous DNA damage and subsequently increase the need for DNA repair. Alternatively, other DNA repair mechanisms might compensate for the loss of BRCA1 in IFE and SG SCs. It has been demonstrated recently that loss of 53BP1 rescues BRCA1 deficiency by re-enabling HR (Bouwman et al. 2010; Bunting et al. 2010). However, the similar levels of 53BP1 expression in the IFE and SG suggest that differential expression of 53BP1 in distinct epidermal SCs is not the primary mechanism underlying the differential sensitivity of these different SC populations to *Brca1* deletion. Future studies will be required to determine whether other components of HR and NHEJ that are able to restore HR in the absence of BRCA1, such as RAD51 (Martin et al. 2007), are differentially expressed in the distinct epidermal compartments, thereby contributing to the specific requirement of BRCA1 in the HF lineages.

BRCA1 is a multifunctional protein involved in different aspects of the DNA damage response, such as DNA repair, checkpoint control, DSB resection, ubiquitination, and chromatin remodeling (Starita and Parvin 2003; Huen et al. 2010; Roy et al. 2012). Interestingly, BRCA1, when partnered with BARD1, controls centrosome numbers through monoubiquitination of γ-tubulin (Xu et al. 1999; Starita et al. 2004) and mitotic spindle assembly (Joukov et al. 2006). It is thus possible that other BRCA1 functions besides HR might be required in HF matrix cells to sustain their proliferation and prevent their apoptosis. Finally, BRCA1 may contribute to the maintenance of the heterochromatin and subsequent gene silencing (Zhu et al. 2011).

Analysis of the heterochromatin and the normally repressed genes might reveal whether this function of BRCA1 plays any critical role in the renewal or differentiation of the HF lineages. Further studies, including genomic and proteomic analyses, will be helpful to discriminate between these different possibilities.

BRCA1 is one of the two main genes associated with familial breast cancer. Germline mutations in *BRCA1* lead to a major increase in the incidence of breast and ovarian cancers, while other epithelia expressing BRCA1 do not show increased tumor formation (Venkitaraman 2009). Our study, demonstrating that certain SCs are lost upon homozygous *Brca1* deletion and consequentially cannot induce cancer formation unless *p53* is concomitantly deleted, provides a possible explanation for this important question. Moreover, understanding the molecular basis of the differential sensitivity of distinct types of SCs to *Brca1* deletion will also be important to define the molecular mechanisms of tissue degeneration and will open the path for the development of new therapies for *BRCA1*-related cancers.

Materials and methods

Mice

Brca1$^{fl/fl}$ (Liu et al. 2007) and *p53*$^{fl/fl}$ (Jonkers et al. 2001) mice were obtained from the National Cancer Institute at Frederick. *Rosa-YFP* mice (Srinivas et al. 2001) were obtained from Jackson Laboratory. *K14Cre* (Vasioukhin et al. 1999) and *TRE-mCMV-H2B-GFP* (Tumbar et al. 2004) mice were a kind gift from E. Fuchs (Howard Hughes Medical Institute, The Rockefeller University, New York). *K5tTA* mice (Diamond et al. 2000) were a kind gift from A. Glick (Laboratory of Cellular Carcinogenesis and Tumor Promotion, National Cancer Institute, Bethesda, MD). The *K5CreER* mice were a kind gift from B. Hogan (Department of Cell Biology, Duke University Medical Center, Durham, NC). All animal experiments were performed in accordance with the guidelines of the Free University of Brussels (ULB) and the Ethical Committee for Animal Welfare (reference no. 260N).

Animal treatments

The pan-caspase inhibitor Z-VAD-FKM was injected intraperitoneally daily at 10 μg/g body weight to pregnant females from E10 to E17.

To perform proliferation studies, BrdU (Sigma-Aldrich) was injected intraperitoneally at 50 mg/kg twice daily for 24 h for the proliferation analyses and from P3 to P5 for the label retention studies. Doxycycline was administered to pregnant and lactating female *K5tTA;TetO-H2B-GFP* and *K5tTA;TetO-H2B-GFP;K14Cre;Brca1*$^{fl/fl}$ mice in food pellets, starting at E18.5.

K5CreER;Brca1$^{fl/fl}$*;Rosa-YFP* mice were injected intraperitoneally with 2.5 mg of TAM every other day until a total dose of 15 mg.

Antibodies

For immunofluorescence, the following antibodies were used: anti-P-Cadherin (rat, 1:200; Zymed); anti-GFP (rabbit, 1:1000; Abcam); anti-β4 integrin (rat, 1:200; BD Biosciences); anti-K14 (chicken, 1:10,000; Covance); anti-K10 (rabbit, 1:1000; Covance); anti-K1 (rabbit, 1:1000; Covance); anti-Loricrin (rabbit, 1:1000; Covance); anti-Lrig1 (goat, 1:1000; R&D Systems); anti-Gata3 (mouse, 1:100; Santa Cruz Biotechnology); anti-Lhx2 (1:500; Santa Cruz Biotechnology); anti-Dsc2 (1:50; Santa Cruz Biotechnology); anti-BrdU (rat, 1:400; Abcam); anti-active caspase-3 (rabbit, 1:600; R&D Systems); anti-CD34 (rat, 1:100; eBiosciences); anti-γH2AX (mouse, 1:600; Millipore); anti-53BP1 (rabbit, 1:500; Novus Biological); anti-AE13, anti-AE15, and anti-Nfatc1 (all 1:100; Abcam); anti-β-catenin (1:500; Abcam); anti-rat, anti-mouse, anti-goat, anti-chicken, and anti-rabbit conjugated with Alexa-488 (all donkey, 1:400; Invitrogen); and anti-rat and rabbit conjugated with RRX (donkey, 1:400; Jackson Immunoresearch). Anti-MTS24 (1:200) was a kind gift from Richard Boyd (Monash Immunology and Stem Cell). Rabbit antiserum to NPNT was generated as described previously (Sato et al. 2009).

The mouse monoclonal anti-mouse BRCA1 antibody (mBRCA1-16588) was raised against a C-terminal fragment of the mouse BRCA1 protein. A construct encoding residues 1328–1821 was kindly provided by Stoil Dimitrov and David Livingston (Dana Farber Cancer Institute, Harvard Medical School, Boston) and recloned into the GST-LIC vector pGEXNKI-GST-3C-LIC (Luna-Vargas et al. 2011) to allow recombinant protein purification. Purified protein was used to generate mouse hybridoma cell lines (BioGenes).

For FACS analysis, the following antibodies were used: biotinylated anti-CD34 (1:50; EBiosciences), PE-conjugated anti-α6 integrin (1:50), FITC-conjugated anti-BrdU (1:50), and APC-conjugated streptavidin (1:400; all by BD Biosciences).

For Western blot, we used the following antibodies: anti-γH2AX (1:1000; Millipore) and anti-actin (1:1000; Abcam).

Immunofluorescence

Paraffin sections were performed and stained as previously described (Sotiropoulou et al. 2010). Antigen unmasking was performed in the PT module (LabVision) for 20 min at 98°C using citrate buffer (pH 6.0; LabVision).

Frozen sections from cryopreserved tissue, embedded in cryomold (Sakura) using OCT (Tissue Tek), were performed on Superfrost slides (Menzel GmbH) using a cryostat CM-3050-S (Leica) and were fixed for 10 min in paraformaldehyde 4% in PBS. Nonspecific antibody binding was prevented by blocking with 5% horse serum (HS), 1% BSA, and 0.2% Triton X-100 for 1 h at room temperature. When mouse primary antibodies were used, nonspecific antigen blocking was performed using the M.O.M. Basic kit reagent (Vector Laboratories) according to the manufacturer's instructions. Slides were then incubated overnight at 4°C in the presence of the primary antibodies, followed by 1 h of incubation of the secondary antibodies at room temperature. Slides were mounted using Glycergel (Dako) supplemented with 2.5% DABCO (Sigma-Aldrich).

For γH2AX immunofluorescence, the following modifications from the above protocol were made: The cryosections were fixed for 20 min in 2% paraformaldehyde in PBS and, upon washing, were incubated in 70% ethanol for 20 min at −20°C. Nonspecific antibody binding was prevented by blocking with 8% BSA, 0.5% Tween 20, and 0.1% Triton X-100 for 1 h at room temperature.

Immunohistochemistry

For p53, 4-μm paraffin sections were deparaffinized and rehydrated. For *Brca1*, cryosections were used. The antigen unmasking procedure was performed for 20 min at 98°C in citrate buffer (pH 6) using the PT module. Endogenous peroxydase was blocked using 3% H_2O_2 (Merck) in methanol (VWR) for 10 min at room

temperature. Endogenous avidin and biotin were blocked using the Endogenous Blocking kit (Invitrogen) for 20 min at room temperature. In p53 staining, nonspecific antigen blocking was performed using M.O.M. Basic kit reagent. Mouse anti-p53 antibody (clone 1C12; Cell Signaling) was incubated overnight at 4°C. Anti-mouse biotinylated in M.O.M. Blocking kit, Standard ABC kit, and ImmPACT DAB (Vector Laboratories) was used for the detection of HRP activity. Slides were then dehydrated and mounted using SafeMount (Labonord).

Oil Red O staining

Oil Red O staining was performed by 30 sec of incubation in Oil Red O of cryosections previously fixed with 4% PAF for 10 min and permeabilized with 60% isopropanol for 5 min. Slides were thoroughly washed with tap water, stained with Mayer's hematoxylin for 2 min, washed with water, and mounted.

Image acquisition

Imaging was performed on a Zeiss Axio Imager.M1 (Thornwood) fluorescence microscope with a Zeiss Axiocam MRm camera for immunofluorescence microscopy and a Zeiss Axioxam MRC5 camera for bright-field microscopy using Axiovision release 4.6 software. Confocal images were acquired at room temperature using a Zeiss LSM780 multiphoton confocal microscope fitted on an Axiovert M200 inverted microscope equipped with C-Apochromat (40×, NA 1.2) water immersion objectives (Carl Zeiss, Inc.). Optical sections of 1024 × 1024 pixels were collected sequentially for each fluorochrome. The data sets generated were merged and displayed with the ZEN software. Photoshop CS3 (Adobe) was used to adjust brightness, contrast, and picture size.

Flow cytometry and cell sorting

For flow cytometry, isolation of keratinocytes and bulge SCs was performed as previously described (Sotiropoulou et al. 2010). FACS analysis for cell proliferation was performed using the BrdU Flow kit (BD Biosciences). Dead cells were excluded using Hoechst 33342 at 4 μM. FACS analysis was performed using LSR Fortessa and FACS DiVa software (BD Biosciences). For cell sorting, IFE and HF cells were isolated as previously described (Lichti et al. 2008). The FACSAria cell sorter (BD Biosciences) and FACS DiVa software were used for cell sorting.

Western blot analysis

FACS-sorted cells (10^5) were lysed in 50 μL of laemli lysis buffer for 10 min at 100°C and sonicated at 30% amplitude seven times for 2 sec each. Subsequently, 30 μL of lysate was loaded on a 10% acrylamide/bis-acrylamide gel (Invitrogen). Proteins were then transferred on PVDF membranes. ECL anti-mouse IgG conjugated with horseradish peroxidase (1:10,000; Healthcare) was used as the secondary antibody.

Quantitative PCR

DNA purification from FACS-sorted cells was performed using the DNeasy blood and tissue kit (Qiagen). quantitative PCR analyses were performed using a Quantifast SYBR Green mix (Qiagen) on an Agilent Technologies Stratagene Mx3500P real-time PCR system. β-Actin was used as the housekeeping internal reference gene. The primers and conditions used were previously described (Liu et al. 2007). Specificity of the PCR amplification was assessed by electrophoresis of the amplicons on 2% agarose gels.

Statistical analysis

Statistical significance was computed using Student's *t*-test statistics.

Acknowledgments

We thank J.-M. Vanderwinden for his help with bioimaging, T. Karagiannis for the protocol of γH2AX staining on skin tissue, Christine Dubois for cell sorting, and Cecile Denaux for technical help. We also thank the NKI Protein Facility for assistance with antibody purification. P.A.S. is chercheur qualifie of the FRS/FNRS. A.K. is an aspirant FRS/FNRS. A.C. is a research fellow of the FRS/FRIA. C.B. is an investigator of WELBIO. This work was supported by the FNRS, TELEVIE, the Program D'Excellence CIBLES of the Wallonia Region, a research grant from the Fondation Contre le Cancer, the ULB Fondation, the Fond Gaston Ithier, a starting grant of the European Research Council (ERC), and the EMBO Young Investigator Program.

References

Birbeck MS, Mercer EH. 1957. The electron microscopy of the human hair follicle. III. The inner root sheath and trichohyaline. *J Biophys Biochem Cytol* **3:** 223–230.

Blanpain C, Fuchs E. 2006. Epidermal stem cells of the skin. *Annu Rev Cell Dev Biol* **22:** 339–373.

Blanpain C, Fuchs E. 2009. Epidermal homeostasis: A balancing act of stem cells in the skin. *Nat Rev Mol Cell Biol* **10:** 207–217.

Blanpain C, Lowry WE, Geoghegan A, Polak L, Fuchs E. 2004. Self-renewal, multipotency, and the existence of two cell populations within an epithelial stem cell niche. *Cell* **118:** 635–648.

Blanpain C, Mohrin M, Sotiropoulou PA, Passegue E. 2011. DNA-damage response in tissue-specific and cancer stem cells. *Cell Stem Cell* **8:** 16–29.

Bonner WM, Redon CE, Dickey JS, Nakamura AJ, Sedelnikova OA, Solier S, Pommier Y. 2008. γH2AX and cancer. *Nat Rev Cancer* **8:** 957–967.

Bouwman P, Aly A, Escandell JM, Pieterse M, Bartkova J, van der Gulden H, Hiddingh S, Thanasoula M, Kulkarni A, Yang Q, et al. 2010. 53BP1 loss rescues BRCA1 deficiency and is associated with triple-negative and BRCA-mutated breast cancers. *Nat Struct Mol Biol* **17:** 688–695.

Bunting SF, Callen E, Wong N, Chen HT, Polato F, Gunn A, Bothmer A, Feldhahn N, Fernandez-Capetillo O, Cao L, et al. 2010. 53BP1 inhibits homologous recombination in Brca1-deficient cells by blocking resection of DNA breaks. *Cell* **141:** 243–254.

Cao L, Li W, Kim S, Brodie SG, Deng CX. 2003. Senescence, aging, and malignant transformation mediated by p53 in mice lacking the Brca1 full-length isoform. *Genes Dev* **17:** 201–213.

Chapman JR, Sossick AJ, Boulton SJ, Jackson SP. 2012. BRCA1-associated exclusion of 53BP1 from DNA damage sites underlies temporal control of DNA repair. *J Cell Sci* **125:** 3529–3534.

Clayton E, Doupe DP, Klein AM, Winton DJ, Simons BD, Jones PH. 2007. A single type of progenitor cell maintains normal epidermis. *Nature* **446:** 185–189.

Diamond I, Owolabi T, Marco M, Lam C, Glick A. 2000. Conditional gene expression in the epidermis of transgenic mice using the tetracycline-regulated transactivators tTA and rTA linked to the keratin 5 promoter. *J Invest Dermatol* **115:** 788–794.

Fujiwara H, Ferreira M, Donati G, Marciano DK, Linton JM, Sato Y, Hartner A, Sekiguchi K, Reichardt LF, Watt FM. 2011. The basement membrane of hair follicle stem cells is a muscle cell niche. *Cell* **144:** 577–589.

Garinis GA, van der Horst GT, Vijg J, Hoeijmakers JH. 2008. DNA damage and ageing: New-age ideas for an age-old problem. *Nat Cell Biol* **10:** 1241–1247.

Hakem R. 2008. DNA-damage repair; the good, the bad, and the ugly. *EMBO J* **27:** 589–605.

Harper JW, Elledge SJ. 2007. The DNA damage response: Ten years after. *Mol Cell* **28:** 739–745.

Hoeijmakers JH. 2001. Genome maintenance mechanisms for preventing cancer. *Nature* **411:** 366–374.

Hoeijmakers JH. 2009. DNA damage, aging, and cancer. *N Engl J Med* **361:** 1475–1485.

Horsley V, Aliprantis AO, Polak L, Glimcher LH, Fuchs E. 2008. NFATc1 balances quiescence and proliferation of skin stem cells. *Cell* **132:** 299–310.

Huen MS, Sy SM, Chen J. 2010. BRCA1 and its toolbox for the maintenance of genome integrity. *Nat Rev Mol Cell Biol* **11:** 138–148.

Jensen KB, Collins CA, Nascimento E, Tan DW, Frye M, Itami S, Watt FM. 2009. Lrig1 expression defines a distinct multipotent stem cell population in mammalian epidermis. *Cell Stem Cell* **4:** 427–439.

Jonkers J, Meuwissen R, van der Gulden H, Peterse H, van der Valk M, Berns A. 2001. Synergistic tumor suppressor activity of BRCA2 and p53 in a conditional mouse model for breast cancer. *Nat Genet* **29:** 418–425.

Joukov V, Groen AC, Prokhorova T, Gerson R, White E, Rodriguez A, Walter JC, Livingston DM. 2006. The BRCA1/BARD1 heterodimer modulates ran-dependent mitotic spindle assembly. *Cell* **127:** 539–552.

Lichti U, Anders J, Yuspa SH. 2008. Isolation and short-term culture of primary keratinocytes, hair follicle populations and dermal cells from newborn mice and keratinocytes from adult mice for in vitro analysis and for grafting to immunodeficient mice. *Nat Protoc* **3:** 799–810.

Liu X, Holstege H, van der Gulden H, Treur-Mulder M, Zevenhoven J, Velds A, Kerkhoven RM, van Vliet MH, Wessels LF, Peterse JL, et al. 2007. Somatic loss of BRCA1 and p53 in mice induces mammary tumors with features of human BRCA1-mutated basal-like breast cancer. *Proc Natl Acad Sci* **104:** 12111–12116.

Lombard DB, Chua KF, Mostoslavsky R, Franco S, Gostissa M, Alt FW. 2005. DNA repair, genome stability, and aging. *Cell* **120:** 497–512.

Luna-Vargas MP, Christodoulou E, Alfieri A, van Dijk WJ, Stadnik M, Hibbert RG, Sahtoe DD, Clerici M, Marco VD, Littler D, et al. 2011. Enabling high-throughput ligation-independent cloning and protein expression for the family of ubiquitin specific proteases. *J Struct Biol* **175:** 113–119.

Martin RW, Orelli BJ, Yamazoe M, Minn AJ, Takeda S, Bishop DK. 2007. RAD51 up-regulation bypasses BRCA1 function and is a common feature of BRCA1-deficient breast tumors. *Cancer Res* **67:** 9658–9665.

Mascre G, Dekoninck S, Drogat B, Youssef KK, Brohee S, Sotiropoulou PA, Simons BD, Blanpain C. 2012. Distinct contribution of stem and progenitor cells to epidermal maintenance. *Nature* **489:** 257–262.

Milyavsky M, Gan OI, Trottier M, Komosa M, Tabach O, Notta F, Lechman E, Hermans KG, Eppert K, Konovalova Z, et al. 2010. A distinctive DNA damage response in human hematopoietic stem cells reveals an apoptosis-independent role for p53 in self-renewal. *Cell Stem Cell* **7:** 186–197.

Mohrin M, Bourke E, Alexander D, Warr MR, Barry-Holson K, Le Beau MM, Morrison CG, Passegue E. 2010. Hematopoietic stem cell quiescence promotes error-prone DNA repair and mutagenesis. *Cell Stem Cell* **7:** 174–185.

Nijhof JG, Braun KM, Giangreco A, van Pelt C, Kawamoto H, Boyd RL, Willemze R, Mullenders LH, Watt FM, de Gruijl FR, et al. 2006. The cell-surface marker MTS24 identifies a novel population of follicular keratinocytes with characteristics of progenitor cells. *Development* **133:** 3027–3037.

Nowak JA, Polak L, Pasolli HA, Fuchs E. 2008. Hair follicle stem cells are specified and function in early skin morphogenesis. *Cell Stem Cell* **3:** 33–43.

O'Guin WM, Sun TT, Manabe M. 1992. Interaction of trichohyalin with intermediate filaments: Three immunologically defined stages of trichohyalin maturation. *J Invest Dermatol* **98:** 24–32.

Pulvers JN, Huttner WB. 2009. Brca1 is required for embryonic development of the mouse cerebral cortex to normal size by preventing apoptosis of early neural progenitors. *Development* **136:** 1859–1868.

Rhee H, Polak L, Fuchs E. 2006. Lhx2 maintains stem cell character in hair follicles. *Science* **312:** 1946–1949.

Riley T, Sontag E, Chen P, Levine A. 2008. Transcriptional control of human p53-regulated genes. *Nat Rev Mol Cell Biol* **9:** 402–412.

Rottenberg S, Nygren AO, Pajic M, van Leeuwen FW, van der Heijden I, van de Wetering K, Liu X, de Visser KE, Gilhuijs KG, van Tellingen O, et al. 2007. Selective induction of chemotherapy resistance of mammary tumors in a conditional mouse model for hereditary breast cancer. *Proc Natl Acad Sci* **104:** 12117–12122.

Roy R, Chun J, Powell SN. 2012. BRCA1 and BRCA2: Different roles in a common pathway of genome protection. *Nat Rev Cancer* **12:** 68–78.

Sancar A, Lindsey-Boltz LA, Unsal-Kacmaz K, Linn S. 2004. Molecular mechanisms of mammalian DNA repair and the DNA damage checkpoints. *Annu Rev Biochem* **73:** 39–85.

Sato Y, Uemura T, Morimitsu K, Sato-Nishiuchi R, Manabe R, Takagi J, Yamada M, Sekiguchi K. 2009. Molecular basis of the recognition of nephronectin by integrin α8β1. *J Biol Chem* **284:** 14524–14536.

Schultz LB, Chehab NH, Malikzay A, Halazonetis TD. 2000. p53 binding protein 1 (53BP1) is an early participant in the cellular response to DNA double-strand breaks. *J Cell Biol* **151:** 1381–1390.

Snippert HJ, Haegebarth A, Kasper M, Jaks V, van Es JH, Barker N, van de Wetering M, van den Born M, Begthel H, Vries RG, et al. 2010. Lgr6 marks stem cells in the hair follicle that generate all cell lineages of the skin. *Science* **327:** 1385–1389.

Sotiropoulou PA, Blanpain C. 2012. Development and homeostasis of the skin epidermis. *Cold Spring Harb Perspect Biol* **4:** a008383.

Sotiropoulou PA, Candi A, Mascre G, De Clercq S, Youssef KK, Lapouge G, Dahl E, Semeraro C, Denecker G, Marine JC, et al. 2010. Bcl-2 and accelerated DNA repair mediates resistance of hair follicle bulge stem cells to DNA-damage-induced cell death. *Nat Cell Biol* **12:** 572–582.

Srinivas S, Watanabe T, Lin CS, William CM, Tanabe Y, Jessell TM, Costantini F. 2001. Cre reporter strains produced by targeted insertion of EYFP and ECFP into the ROSA26 locus. *BMC Dev Biol* **1:** 4.

Starita LM, Parvin JD. 2003. The multiple nuclear functions of BRCA1: Transcription, ubiquitination and DNA repair. *Curr Opin Cell Biol* **15:** 345–350.

Starita LM, Machida Y, Sankaran S, Elias JE, Griffin K, Schlegel BP, Gygi SP, Parvin JD. 2004. BRCA1-dependent ubiquitina-

tion of γ-tubulin regulates centrosome number. *Mol Cell Biol* **24:** 8457–8466.

Symington LS, Gautier J. 2011. Double-strand break end resection and repair pathway choice. *Annu Rev Genet* **45:** 247–271.

Trempus CS, Morris RJ, Bortner CD, Cotsarelis G, Faircloth RS, Reece JM, Tennant RW. 2003. Enrichment for living murine keratinocytes from the hair follicle bulge with the cell surface marker CD34. *J Invest Dermatol* **120:** 501–511.

Tumbar T, Guasch G, Greco V, Blanpain C, Lowry WE, Rendl M, Fuchs E. 2004. Defining the epithelial stem cell niche in skin. *Science* **303:** 359–363.

Vasioukhin V, Degenstein L, Wise B, Fuchs E. 1999. The magical touch: Genome targeting in epidermal stem cells induced by tamoxifen application to mouse skin. *Proc Natl Acad Sci* **96:** 8551–8556.

Vasioukhin V, Bauer C, Degenstein L, Wise B, Fuchs E. 2001. Hyperproliferation and defects in epithelial polarity upon conditional ablation of α-catenin in skin. *Cell* **104:** 605–617.

Venkitaraman AR. 2009. Linking the cellular functions of BRCA genes to cancer pathogenesis and treatment. *Annu Rev Pathol* **4:** 461–487.

Xu X, Weaver Z, Linke SP, Li C, Gotay J, Wang XW, Harris CC, Ried T, Deng CX. 1999. Centrosome amplification and a defective G2–M cell cycle checkpoint induce genetic instability in BRCA1 exon 11 isoform-deficient cells. *Mol Cell* **3:** 389–395.

Zhu Q, Pao GM, Huynh AM, Suh H, Tonnu N, Nederlof PM, Gage FH, Verma IM. 2011. BRCA1 tumour suppression occurs via heterochromatin-mediated silencing. *Nature* **477:** 179–184.